BIOCHEMISTRY
including biophysical chemistry & molecular biology

Article

pubs.acs.org/biochemistry

Evidence for a Dual Role of an Active Site Histidine in α-Amino-β-carboxymuconate-ε-semialdehyde Decarboxylase

Lu Huo,[†] Andrew J. Fielding,[‡] Yan Chen,[†] Tingfeng Li,[§,⊥] Hiroaki Iwaki,[∥] Jonathan P. Hosler,[§] Lirong Chen,[†] Yoshie Hasegawa,[∥] Lawrence Que, Jr.,[‡] and Aimin Liu*[,†,§]

[†]Department of Chemistry and Center for Diagnostics and Therapeutics, Georgia State University, P.O. Box 4098, Atlanta, Georgia 30303, United States

[‡]Department of Chemistry and Center for Metals in Biocatalysis, University of Minnesota, 207 Pleasant Street, Minneapolis, Minnesota 55455, United States

[§]Department of Biochemistry, University of Mississippi Medical Center, Jackson, Mississippi 39216, United States

[∥]Department of Life Science and Biotechnology and ORDIST, Kansai University, Suita, Osaka 564-8680, Japan

Supporting Information

ABSTRACT: The previously reported crystal structures of α-amino-β-carboxymuconate-ε-semialdehyde decarboxylase (ACMSD) show a five-coordinate Zn(II)(His)$_3$(Asp)(OH$_2$) active site. The water ligand is H-bonded to a conserved His228 residue adjacent to the metal center in ACMSD from *Pseudomonas fluorescens* (*Pf*ACMSD). Site-directed mutagenesis of His228 to tyrosine and glycine in this study results in a complete or significant loss of activity. Metal analysis shows that H228Y and H228G contain iron rather than zinc, indicating that this residue plays a role in the metal selectivity of the protein. As-isolated H228Y displays a blue color, which is not seen in wild-type ACMSD. Quinone staining and resonance Raman analyses indicate that the blue color originates from Fe(III)-tyrosinate ligand-to-metal charge transfer. Co(II)-substituted H228Y ACMSD is brown in color and exhibits an electron paramagnetic resonance spectrum showing a high-spin Co(II) center with a well-resolved ^{59}Co ($I = {}^7/_2$) eight-line hyperfine splitting pattern. The X-ray crystal structures of as-isolated Fe-H228Y (2.8 Å) and Co-substituted (2.4 Å) and Zn-substituted H228Y (2.0 Å resolution) support the spectroscopic assignment of metal ligation of the Tyr228 residue. The crystal structure of Zn−H228G (2.6 Å) was also determined. These four structures show that the water ligand present in WT Zn-ACMSD is either missing (Fe-H228Y, Co-H228Y, and Zn-H228G) or disrupted (Zn-H228Y) in response to the His228 mutation. Together, these results highlight the importance of His228 for *Pf*ACMSD's metal specificity as well as maintaining a water molecule as a ligand of the metal center. His228 is thus proposed to play a role in activating the metal-bound water ligand for subsequent nucleophilic attack on the substrate.

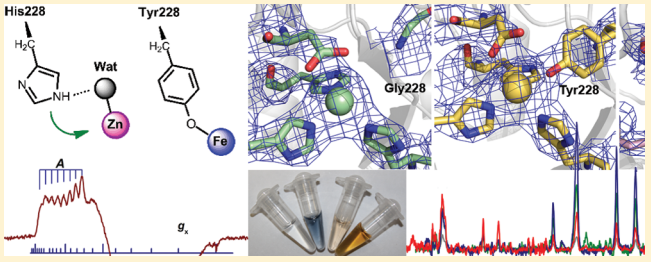

Histidine, an essential amino acid, is found at the active site of a myriad of enzymes. The imidazole side chain of histidine can serve as a coordinating ligand in metalloproteins and in many cases is a catalytically important component in the active sites of enzymes. The pK_a of the imidazolium ion (~7) permits significant concentrations of both acidic and basic forms near neutral pH, making it a commonly found general acid−base catalyst in enzymes.[1] The participation of histidine in catalysis has also been illustrated in the well-studied mechanisms proposed for members of the amidohydrolase superfamily.[2,3] The best-characterized members of the amidohydrolase superfamily share a common catalytic mechanism by which a metal-bound water is proposed to be activated by an active site base to yield a metal-hydroxo species. Subsequently, the hydroxide attacks the substrate bearing the amide or other functional groups at the carbon or phosphorus center to form a tetrahedral carbon or pentacoordinate phosphorus intermediate on the substrate.[2] The collapse of the substrate-based intermediate leads to the hydrolytic products.

The enzyme α-amino-β-carboxymuconate-ε-semialdehyde decarboxylase (ACMSD) catalyzes the decarboxylation of its substrate ACMS to form the 2-aminomuconate semialdehyde (AMS) product. It is the first enzyme known to perform an O$_2$-independent nonoxidative decarboxylation with *d*-block divalent metal cofactors such as zinc, cobalt, and iron.[4] ACMSD is proposed to be a prototypical member of a new protein subfamily in the amidohydrolase superfamily, representing a novel nonhydrolytic C−C bond breaking activity.[5,6] Scheme 1 outlines a working mechanism of the ACMSD catalytic cycle.

Received: May 16, 2012
Revised: June 29, 2012
Published: July 2, 2012

dx.doi.org/10.1021/bi300635b | *Biochemistry* 2012, 51, 5811−5821

Scheme 1. Proposed Catalytic Role of His228 in the ACMSD Reaction

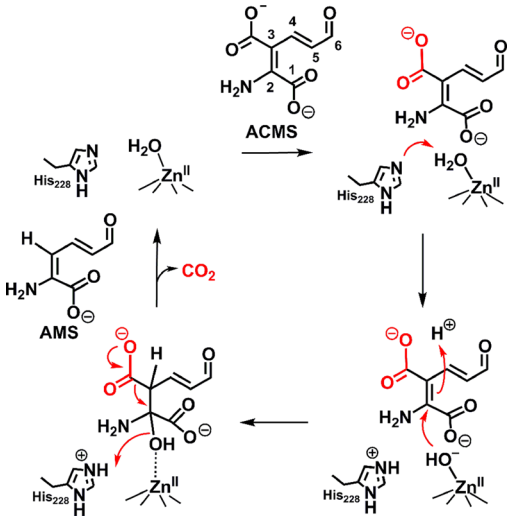

ACMSD plays an important role in two distinct metabolic pathways, the mammalian kynurenine pathway for tryptophan degradation[7] and the bacterial 2-nitrobenzoic acid pathway for biodegradation of nitroaromatic compounds.[8−10] In both pathways, ACMSD controls the final fate of the metabolites by competing with a slow spontaneous reaction that produces the excitotoxin quinolinic acid (QA) and directs the metabolic flux away from QA to energy production.[11] QA is an endogenous selective agonist of *N*-methyl-D-aspartate receptors.[12] It modulates neurotransmission and mediates immune tolerance. Reduced activity of ACMSD can lead to an abnormal QA concentration in body fluids, which has been linked to numerous diseases, including diabetes,[11] neuropsychiatric diseases,[13] neurodegenerative disorders such as Alzheimer's disease and Huntington's disease,[14,15] stroke, and epilepsy.[12,16] Therefore, the results of the mechanistic study of ACMSD have significant medical implications.

Although ACMSD was discovered more than 55 years ago,[17] little was known about the catalytic mechanism until our recent collaborative studies of *Pseudomonas fluorescens* ACMSD (*Pf*ACMSD)[4] unmasked its metal cofactor and determined its three-dimensional structure.[18] The as-isolated enzyme contains a zinc ion,[18] and it works equally well when substituted with a cobalt(II) ion.[4,5] The decarboxylation is rapid (>500 s^{-1}); the release of the product from the active site is the rate-limiting step.[19] Recently, the crystal structure of human ACMSD was reported with a bound inhibitor 1,3-dihydroxyacetonephosphate.[20] Human ACMSD and *Pf*ACMSD present a nearly identical overall structure consisting of an $(\alpha/\beta)_8$-barrel core and a five-coordinate protein-bound zinc ion.[18,20] The metal ion is bound to the enzyme by three histidine residues (His9, His11, and His177), one aspartic acid residue (Asp294), and one water ligand. A nearby histidine from β-strand 6, i.e., His228 in *Pf*ACMSD residue numbering, is located in the secondary sphere and is part of a hydrogen-bonded system that appears to facilitate deprotonation of the water ligated to the catalytic zinc (Figure 1). A comprehensive biochemical, spectroscopic, and structural study presented in this work suggests that His228 is a major determinant of metal preference in *Pf*ACMSD and that it plays an important role in maintaining the hydrolytic water ligand necessary for the decarboxylase chemistry in this enzyme.

EXPERIMENTAL PROCEDURES

Site-Directed Mutagenesis. The plasmid containing His-tagged ACMSD from *P. fluorescens* was used as a template for construction of all of the mutants.[5] The forward primers used in site-directed mutagenesis are 5′-CAA-GATCTGTTTCGGGggTGGTGGGGGAAGTTTCG-3′ for H228G and 5′-CAAGATCTGTTTCGGGtATGGTGGGG-GAAGTTTCG-3′ for H228Y. ACMSD mutants were constructed by the polymerase chain reaction overlap extension mutagenesis technique.[21] The insertion of each construct was verified by DNA sequencing to ensure that base alterations were introduced correctly as expected with no undesired changes. After sequencing, the positive clone was used for overexpression of these mutants in *Escherichia coli* BL21(DE3).

Bacterial Growth and Protein Preparation. The expression and purification of WT *Pf*ACMSD and its mutants were the same as described previously.[5] Apo H228G was prepared by EDTA treatment; Zn(II)-containing H228G proteins were prepared by the metal reconstitution reaction as previously described.[4] Because iron cannot be removed from as-isolated H228Y by a high concentration of EDTA, Zn(II)- and Co(II)-H228Y proteins were obtained by substituting 0.1 mM $CoCl_2$ or $ZnCl_2$ with M9 medium prior to the addition of IPTG for induction during cell culture. The protein was purified in the presence of 0.1 mM $CoCl_2$ or $ZnCl_2$ during the affinity chromatographic step by using a Co(II)- or Zn(II)-charged IMAC column, respectively.

Metal Analysis. The metal content of the as-isolated ACMSD from LB was determined by inductively coupled plasma optical emission spectroscopy (ICP-OES) using a Spectro Genesis spectrometer (Spectro Analytical Instruments). Assays were performed in triplicate for the mutants

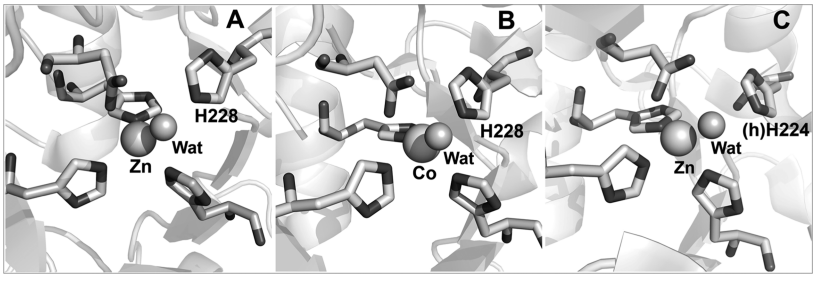

Figure 1. Active site histidine (His228 or His224) within H-bonding distance with the metal-bound water ligand (Wat) in crystal structures of ACMSD. (A) As-isolated Zn-*Pf*ACMSD (PDB entry 2HBV),[18] (B) Co(II)-substituted *Pf*ACMSD (PDB entry 2HBX),[18] and (C) an inhibitor-bound structure of human ACMSD (PDB entry 2WM1).[20]

dx.doi.org/10.1021/bi300635b | *Biochemistry* 2012, 51, 5811−5821

the same day as the assay samples of the wild-type (WT) enzyme. Standard curves were prepared using a transition element standard mixture (CCS-6) from Inorganic Ventures. The error (standard deviation) of three measurements of each sample was less than 1%, while the error between different ACMSD preparations was less than 4%. The metal content is reported per ACMSD monomer. The protein concentration was measured using Coomassie Plus protein assay reagent (Pierce) according to the manufacturer's instructions. The molar concentration of the *Pf*ACMSD monomer was determined by using 39 kDa as the molecular mass.[4]

Circular Dichroism Spectroscopy. The CD spectra (190−250 nm) of ACMSD and mutant proteins were acquired on a JASCO J-810 spectropolarimeter (JASCO, Easton, MD) at ambient temperature. In each measurement, a protein sample (10 μM) was placed in a 1 mm path length quartz cell in 0.05 M potassium phosphate (pH 7.5). All spectra were the average of 10 scans with a scan rate of 50 nm/min.

Preparation of ACMS and Enzyme Activity Assay. ACMS was generated from 3-hydroxyanthranilic acid using 3-hydroxyanthranilate 3,4-dioxygenase containing no free transient metal ion as reported previously.[5] Specific activities of ACMSD proteins were measured in triplicate at room temperature on an Agilent 8453 diode-array spectrophotometer by monitoring the absorbance of ACMS at 360 nm as described previously.[5]

Electronic Spectroscopy. UV−vis absorption spectra were recorded in 25 mM HEPES-NaOH buffer (pH 7.0) and 5% glycerol at room temperature on a Cary 50 spectrophotometer. Reduced Fe(II)-H228Y for UV−vis and resonance Raman experiments was prepared by adding 13 μL of 30 mM sodium dithionite or L-ascorbate (~2 equiv per Fe) to 150 μL of 1.4 mM Fe(III)-H228Y in a 1 mm path length cuvette.

Quinone-Based NBT Staining. Purified proteins were first electrophoresed on a 12% sodium dodecyl sulfate−polyacrylamide gel electrophoresis gel and then transferred onto a nitrocellulose membrane using the Mini Trans-Blot Cell Assembly (Bio-Rad). The transblotting was conducted in transfer buffer (25 mM Tris-HCl, 192 mM glycine, and 20% methanol) at 100 V for 1 h. The proteins were temporarily visualized with 0.1% Ponceau S in 5% acetic acid.[22] After the temporary stains were removed with water, the protein-containing nitrocellulose membrane was immersed in a solution of 0.24 mM NBT and 2 M potassium glycinate (pH 10) in the dark for 45 min to visualize the quinone-containing protein band.[23] This method was designed to identify quinonoid compounds, such as DOPA and is a convenient assay for quinone-containing proteins.[24] Purified methylamine dehydrogenase (MADH) from *Paracoccus denitrificans* (a generous gift from V. L. Davidson), a protein consisting of two large α-subunits and two small β-subunits with a tryptophan tryptophyquinone prosthetic group in each of its small subunits,[25] was used as both a positive and a negative control in Ponceau S staining and NBT staining experiments.

Electronic Paramagnetic Resonance (EPR) Spectroscopy. HEPES buffer (25 mM, pH 7.0) containing 10% glycerol was used in the EPR sample preparations. X-Band EPR spectra were recorded in perpendicular mode on a Bruker (Billerica, MA) EMX spectrometer at a 100 kHz modulation frequency using a 4119HS high-sensitivity resonator. The low temperature was maintained with an ITC503S temperature controller, an ESR910 liquid helium cryostat, and an LLT650/13 liquid helium transfer tube (Oxford Instruments, Concord, MA). Measurements were taken by keeping the frequency of the electromagnetic radiation constant while the magnetic field was swept.

Raman Spectroscopy. Resonance Raman spectra were recorded on an Acton AM-506 spectrophotometer (1200 groove rating) using Kaiser Optical Systems holographic supernotch filters and a Princeton Instruments liquid N_2-cooled CCD detector (LN-1100PB) with a 4 cm^{-1} spectral resolution. HEPES buffer (25 mM, pH 7.0) containing 5% glycerol was used in the sample preparations. Spectra were recorded at a laser power of 100 mW using a Spectra Physics 1060-KR-V krypton ion laser (568.2 and 647.1 nm) or a 2030-15 argon ion laser (488.0 and 514.5 nm). Raman frequencies were referenced to the indene standard with an accuracy of ±1 cm^{-1}. Raman spectra were recorded at 4 °C by 90° scattering from a flat-bottom NMR tube with 30−60 min to collect each window of spectra. The full spectra were collected in two overlapping windows; the fluorescent background was subtracted before the spectra were normalized at the non-resonance-enhanced protein phenylalanine ring vibration of 1004 cm^{-1} and normalized spectra were spliced together. Baseline corrections (polynomial fits) were applied using Gram/32 Spectral Notebook (ThermoGalactic). Excitation profiles were constructed by comparing peak intensities of resonance-enhanced bands of normalized spectra to the non-resonance-enhanced vibration at 1004 cm^{-1}. Difference resonance Raman spectra of Fe(III)-H228Y were obtained by subtracting the spectrum of WT Zn-ACMSD normalized at the 1004 cm^{-1} vibration followed by a baseline correction.

X-ray Data Collection and Crystallographic Refinement. Co(II)-H228Y, Zn(II)-H228Y, and Zn(II)-H228G ACMSD were crystallized using the conditions previously established for WT ACMSD by hanging drop vapor diffusion in VDX plates (Hampton Research). Single crystals suitable for X-ray data collection were obtained from drops assembled with 1 μL of a protein solution layered with 1 μL of a reservoir solution containing 0.1 M Tris-HCl (pH 8.75), 0.2 M $MgCl_2$, and 15% PEG 5000. The reservoir solution for Fe(III)-H228Y was modified and contained 0.1 M Tris (pH 7.0), 0.2 M $MgCl_2$, and 17% PEG 5000. Crystals were frozen in liquid nitrogen after being dipped into the cryoprotectant solution that contained 30% glycerol or ethylene glycol in the mother liquid. X-ray diffraction data were collected on SER-CAT beamline 22-ID or 22-BM of the Advanced Photon Source (APS, Argonne National Laboratory, Argonne, IL). Data were collected at 100 K using a beam size matching the dimensions of the largest crystal face. The data were processed with HKL2000.[26] Structures were determined by molecular replacement using MolRep[27] from the CCP4 program suite[28] with the entire WT Co(II)-ACMSD structure (PDB entry 2HBX) for Co(II)/Fe(III)-H228Y ACMSD and the WT Zn(II)-ACMSD structure (PDB entry 2HBV) for Zn(II)-H228Y/Zn(II)-H228G ACMSD as the search models. Refinement was conducted using REFMAC[29] in the CCP4 program suite[28] for Fe(III)- and Co(II)-H228Y and PHENIX software for Zn(II)-H228Y and Zn(II)-H228G, and model building was conducted in COOT.[30] Restrained refinement was conducted using no distance restraints between the metal center and its ligands. Residues Tyr228 and Gly228 were well-ordered and added to the model based on the $2F_o - F_c$ and $F_o - F_c$ electron density maps. Refinement was assessed as complete when the $F_o - F_c$ electron density contained only noise.

RESULTS

Biochemical Properties of the His228 Mutants. To probe its role in the enzyme mechanism, we mutated His228 to tyrosine, which also has a ring structure and is capable of hydrogen bonding, and glycine, which effectively deletes the side chain and thus eliminates hydrogen bonding. Both variants were expressed as soluble proteins. Surprisingly, the H228Y mutant purified from cells grown in LB medium exhibits a blue chromophore, while wild-type (WT) Zn-ACMSD is colorless (Figure 2). Metal analysis of blue H228Y-ACMSD by ICP-OES

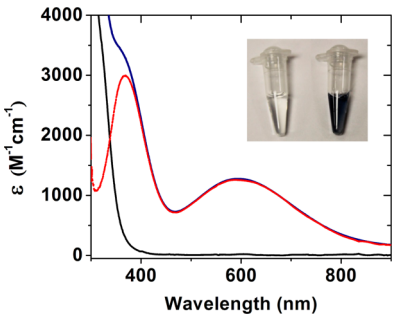

Figure 2. UV−vis spectra of Fe-H228Y: as-isolated Fe(III)-H228Y protein (dark blue), its reduced form (black), and the difference (red) showing two absorptions at 370 nm (3000 M^{-1} cm^{-1}) and 595 nm (1255 M^{-1} cm^{-1}). Photograph of the as-isolated Fe(III)-H228Y (right) and reduced Fe(II)-H228Y (left) are shown in the inset.

spectroscopy showed the enzyme contained 0.51 ± 0.013 Fe, 0.08 ± 0.003 Zn, and 0.001 ± 0.0004 Cu ion per polypeptide chain, whereas the wild-type enzyme prepared under the same experimental conditions contained only zinc.[18] Likewise, the as-isolated H228G mutant contained mainly Fe ion (0.32 ± 0.001 ion per polypeptide chain) and a trace amount of zinc. A sharp ferric EPR signal is seen at g = 4.27 from the two as-isolated His228 mutants (not shown). These results suggest His228 is an important determinant of metal selectivity in this enzyme.

As-isolated H228G and H228Y were catalytically inactive regardless of whether the Fe ion is in the ferrous or ferric oxidation state. Zinc- and cobalt-substituted variants were also tested. H228Y was inactive in both Zn(II) and Co(II) forms, as was Zn(II)-H228G. These results suggest that His228 is essential for the enzyme catalytic activity.

The Blue Color in H228Y Is Not Due to Formation of a Metal-Bound Dihydroxyphenylalanine. Two possibilities were considered for the origin of the blue chromophore of the as-isolated Fe-containing H228Y. The first option is to produce an oxygenated Tyr by post-translational modification resulting from oxygen activation by the redox active iron. Examples can be found for a number of non-heme iron enzymes.[24,31,32] However, this option is not supported by a quinone-based staining assay[24] using reversible Ponceau S staining of a nitrocellulose membrane (see Figure S1 of the Supporting Information). Alternatively, it could be due to the coordination of Tyr228 to the active site metal, as tyrosinate−metal interactions have been observed in many other enzymes, such as purple acid phosphatases,[33] phospholipase D,[34] and catalases.[35]

Resonance Raman Characterization Suggests an Fe(III)-Tyrosinate Chromophore in As-Isolated Fe-H228Y. The blue Fe-H228Y mutant exhibits two UV−vis absorption bands at 370 and 595 nm, with extinction coefficients of 3000 and 1300 M^{-1} cm^{-1}, respectively (Figure 2). While the 370 nm feature is a common spectral characteristic of the Fe(III)-bound non-heme Fe proteins, the blue chromophore at 595 nm is within the range of an iron(III)-tyrosinate ligand-to-metal charge transfer (LMCT) band with an absorption maximum that is typically between 410 and 600 nm (1000−2500 M^{-1} cm^{-1} per phenolate ligand).[36] In contrast, an iron(III)-catecholate LMCT chromophore typically exhibits two lower-energy bands between 400−580 and 550−900 nm (2000−2500 M^{-1} cm^{-1}); these are not present in Figure 2. The blue chromophore vanished upon addition of sodium dithionite or L-ascorbate to the protein, suggesting that reduction of the Fe(III) metal center to Fe(II) is linked with the loss of the intense LMCT transition.

Figure 3A shows resonance Raman spectra of as-isolated blue Fe-H228Y acquired with 568.2 nm laser excitation using 90° scattering geometry compared to the spectra of reduced Fe-H228Y, WT Zn-ACMSD, and the buffer [25 mM HEPES (pH 7.0) with 5% glycerol by volume] collected under the same conditions. Vibrations associated with the buffer solution and protein were subtracted by taking the difference spectrum of as-isolated blue Fe-H228Y and WT Zn-ACMSD after normalizing both spectra by scaling to the non-resonance-enhanced protein phenylalanine ring vibration at 1004 cm^{-1} (Figure 3B). The difference spectrum shows resonance-enhanced vibrations at 573, 792, 873, 1164, 1290, 1503, and 1604 cm^{-1}. The excitation profile of the 1164, 1290, 1503, and 1604 cm^{-1} features shown in Figure 3C illustrates the maximal enhancement of these vibrations near the absorption maximum of the blue chromophore at 595 nm, while the 573, 792, and 873 cm^{-1} vibrations are more enhanced at 647.1 nm. The spectrum of the reduced form of colorless Fe(II)-H228Y does not exhibit any resonance-enhanced vibrations but closely resembles that of WT Zn-ACMSD (Figure 3A).

The resonance-enhanced vibrations of Fe(III)-H228Y at 573, 1164, 1290, 1503, and 1604 cm^{-1} are collectively regarded as the Raman signature for a Fe(III)-tyrosinate chromophore (Table 1).[36−48] These vibrations are distinct from those expected for a Fe(III)-catecholate chromophore, which has characteristic vibrations observed at 1270, 1320, 1425, and 1475 cm^{-1} (Table 1).[49−53] By analogy to previous work on non-heme Fe proteins, the 573 cm^{-1} vibration can be assigned to the Fe-$(O)_{Tyr}$ vibration, while the higher-frequency vibrations are associated with aromatic ring modes. The 792 and 873 cm^{-1} vibrations may originate from a Fermi doublet formed by the mixing of the fundamental υ_1 symmetric ring breathing vibrational mode and first overtone υ_{16a} nonplanar ring vibration.[54−57] Solid L-tyrosine exhibits a Fermi doublet with peaks at 803 and 845 cm^{-1} as well as the υ_{16a} fundamental at 419 cm^{-1}.[55] The two peaks observed for blue Fe-H228Y have a much larger splitting of 81 cm^{-1}. A similarly large splitting has been observed for porcine uteroferrin (803 and 873 cm^{-1}), while the υ_{16a} fundamental was not detected.[54,57] The large splitting of the tyrosine Fermi doublet was rationalized as a result of the strong covalence of the Fe(III)-tyrosinate metal ligand bond based on the fact that it was resonance enhanced and that its center of gravity (~838 cm^{-1}) is similar to that of L-tyrosine (~824 cm^{-1}).[54] Upon 647.1 nm laser excitation of blue Fe-H288Y, a weak peak is observed at 418 cm^{-1} that may be assigned to the fundamental υ_{16a} vibration.

Fe(III)-tyrosinate LMCT bands in the visible region typically range from 410 to 600 nm where the energy of the LMCT transition can be correlated with the Lewis acidity and the

dx.doi.org/10.1021/bi300635b | Biochemistry 2012, 51, 5811−5821

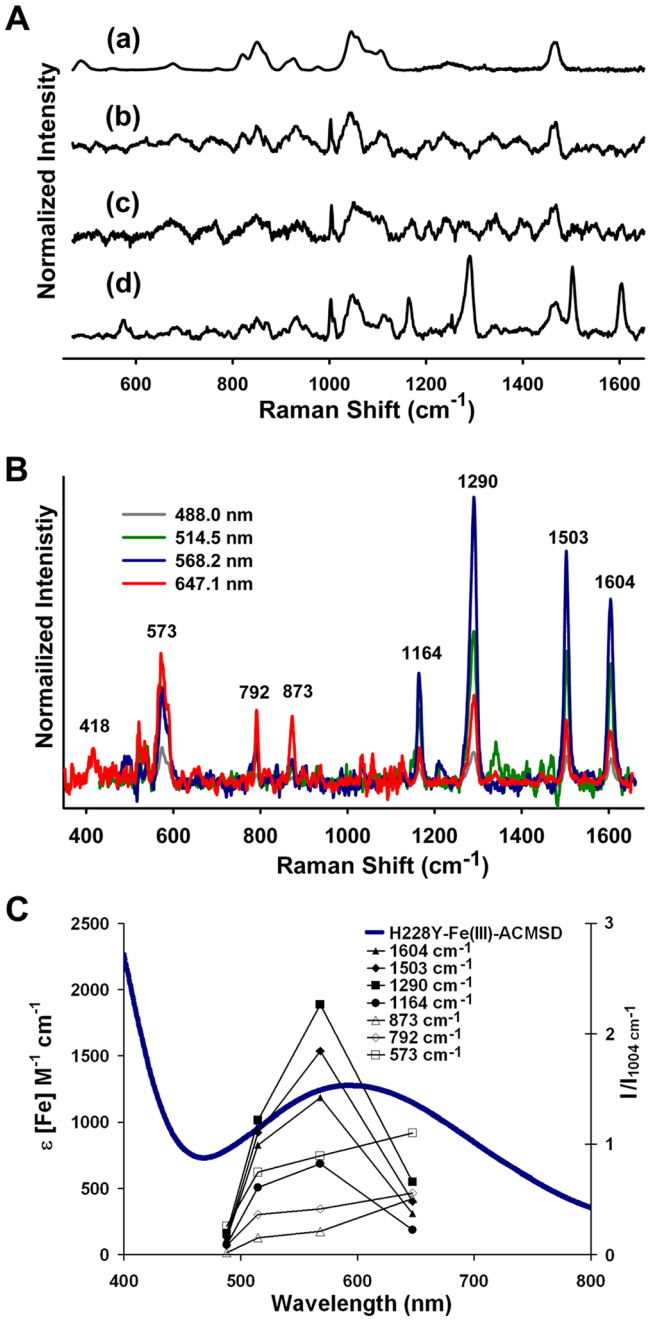

Figure 3. (A) Resonance Raman spectrum with 568.2 nm laser excitation of (a) 25 mM HEPES pH 7.0 with 5% glycerol by volume, (b) native Zn-ACMSD, (c) Fe(II)-H228Y ACMSD, and (d) Fe(III)-H228Y ACMSD. The buffer used for these proteins consisted of 25 mM HEPES (pH 7.0) with 5% glycerol by volume. (B) Difference resonance Raman spectra of Fe(III)-H228, obtained with 488.0, 514.5, 568.2, and 647.1 nm laser lines minus the spectrum of wild-type Zn(II)-ACMSD. The spectra are normalized to the protein phenylalanine ring vibration at 1004 cm^{-1} before subtraction. (C) Excitation profiles for resonance-enhanced bands compared to the extinction coefficient of the Fe(III)-H228Y blue chromophore and colorless reduced Fe(II)-H228Y obtained using 488.0, 514.5, 568.2, and 647.1 nm laser lines.

Fe(III/II) redox potential of the iron center and can give additional information about the nature of the other coordinating ligands.[36] The low energy of the Fe(III)-tyrosinate LMCT band of Fe-H228Y at 595 nm and the observation that Fe-H228Y is easily reduced by mild reducing agents like L-ascorbate are consistent with a Lewis acidic metal center with weak field ligands.[37] Post-translationally modified blue (4-hydroxyphenyl)pyruvate dioxygenase (HPPD) has a similarly low-energy Fe-tyrosinate LMCT band at 595 nm.[37,58] From its crystal structure,[59] unmodified HPPD has an iron center coordinated by two histidines and one glutamate, but no tyrosinate ligand. However, it does have several phenylalanine amino acid residues in the second sphere, one of which has been proposed to be self-hydroxylated to form the tyrosinate ligand in blue HPPD.[53,59] On the basis of the similar energies of their LMCT bands, blue Fe(III)-H228Y and the self-hydroxylated HPPD are likely to have comparable ligand environments with two or three histidine residues and a carboxylate group from either an aspartate or glutamate. Along with the fact that H228Y no longer picks up Zn(II), the Fe(III) is likely to be coordinated by His9, His11, His177, Asp294, and Tyr228 residues in the ACMSD active site.

Spectroscopic Characterization of Co(II)-Substituted H228Y. Co(II)-H228Y was obtained by adding supplemental $CoCl_2$ to the M9 minimum growth medium and purification buffer (see Experimental Procedures). ICP-OES spectroscopic analysis confirmed that H228Y isolated with supplemental cobalt contains 0.98 ± 0.02 cobalt and 0.05 ± 0.03 iron per protein monomer. The cobalt-substituted H228Y displays a brown chromophore that is darker than the WT Co(II)-substituted ACMSD (Figure 4A). The brown chromophore originates from forbidden metal d−d transitions, the intensities of which can be correlated to the metal coordination number.[60] Decreasing the coordination number increases the intensity of the d−d bands due to greater p−d orbital mixing. Typically, six-coordinate high-spin Co(II) complexes have extinction coefficients of <50 M^{-1} cm^{-1} above 500 nm, while five- and four-coordinate complexes have values of 50−250 and >300 M^{-1} cm^{-1}, respectively.[61−63] The visible spectrum of the brown Co(II)-substituted H228Y is similar to that of WT Co(II)-ACMSD above 500 nm (Figure 4A), consistent with a five-coordinate Co(II) center.[64] However, the spectrum below 500 nm is distinct from that of the wild-type protein (Figure 4A). The absorption peaks at 355 nm (680 ± 20 cm^{-1} M^{-1}) and 420 nm (430 ± 10 cm^{-1} M^{-1}) in WT ACMSD are red-shifted to 380 nm (590 ± 30 cm^{-1} M^{-1}) and 458 nm (490 ± 20 cm^{-1} M^{-1}), respectively, in Co(II)-substituted H228Y. These differences indicate that the Co(II) center in the H228Y mutant is in a weaker ligand field environment than in WT Co(II)-substituted ACMSD. This observation is consistent with the substitution of a water ligand by a stronger π-donating ligand in Co(II)-substituted H228Y due to ligation of Tyr228 to the metal as suggested by a resonance Raman study of Fe-H228Y in as-isolated H228Y protein.

Electron paramagnetic resonance (EPR) spectroscopy was employed to characterize the electronic structure of the metal center in Co(II)-substituted H228Y. The EPR spectrum of Co-H228Y exhibits an $S = {}^3/_2$ spectrum with a well-resolved eight-line ^{59}Co hyperfine interaction pattern associated with the low-field feature (Figure 4B), consistent with a high-spin Co(II) ion bound specifically to the protein. An Fe(III) EPR signal is also present at $g = 4.27$, showing that a minor fraction of protein still binds iron even under the cobalt-rich conditions. The well-resolved ^{59}Co hyperfine structure of Co-H228Y can be observed even at 10−20 K, but only a featureless cobalt signal can be observed in WT Co-ACMSD at this temperature.[4] The g value of the high-field feature of the Co-H228Y mutant is also

dx.doi.org/10.1021/bi300635b | Biochemistry 2012, 51, 5811−5821

Table 1. Resonance Raman Vibrations and LMCT Bands of Non-Heme Iron Protein and Model Complexes with Fe(III)-Phenolate and Fe(III)-Catecholate Chromophores

complex[a]	λ_{max} (nm) [ε (M^{-1} cm^{-1})]	resonance Raman vibrations (cm^{-1})									ref
Fe(III)-Phenolate Complexes											
Fe(III)-H228Y-ACMSD	370 (3000), 595 (1255)		573	792	873	1164	1290		1503	1604	this work
Fe(II)-HPPD with O_2	595 (2600)		583	751	881	1171	1290		1502	1600	37, 58
porcine uteroferrin	545 (1000)		575	803	873	1173	1293		1504	1607	54, 57
$[Fe(salhis)_2]ClO_4$	530 (4100)					1159	1337		1476	1625	
						1132	1310		1452	1605	42
Fe(III)-serotransferrin	470 (2500)			759	828	1174	1288		1508	1613	45, 48
Fe(III)-lactoferrin	465 (2070)					1170	1272		1500	1604	46, 47
Fe(III)-ovotransferrin	465 (2000)			759	860	1173	1264		1501	1603	40
catechol 1,2-dioxygenase	450 (3000−4000)			757	872	1175	1289		1506	1604	42, 43
protocatechuate 3,4-dioxygenase	435 (3000), 525		592	756	826	1172	1254		1506	1604	38, 41
					854	1180	1266				
$[Fe(salen)(OC_6H\text{-}4\text{-}CH_3)]$	410		568			1168	1272		1501	1603	36, 44
Fe(III)-Catecholate Complexes											
Fe(III)TyrH-dopamine	415 (1700), 695 (2000)	528	592	631		1275	1320	1425	1475		52
blue PMI	420 (1500), 680 (2100)		591	631		1266	1330	1428	1482		50
Fe(III)-MndD-DOPA	675 (750)	530	569	646	666	1273	1318	1423	1464		73
			586								
Fe(II)TauD-αKG with O_2	550 (700)	544	580	623	644	1261	1314	1425	1475		51, 74

[a]Abbreviations: ACMSD, α-amino-β-carboxymuconate-ε-semialdehyde decarboxylase from *P. fluorescens*; salhis, *N*-[2-(4-imidazolyl)ethyl]-salicylaldimine; salen, *N*,*N*′-ethylenebis(salicylidenamine) dianion; MndD, homoprotocatechuate 2,3-dioxygenase from *Arthrobacter globiformis*; DOPA, dihydroxyphenylalanine; PMI, phosphomannose isomerase from *Candida albicans* expressed in *E. coli*; TauD, taurine/α-ketoglutarate dioxygenase from *E. coli*; HPPD, (4-hydroxyphenyl)pyruvate dioxygenase from *P. fluorescens*; α-KG, α-ketoglutarate.

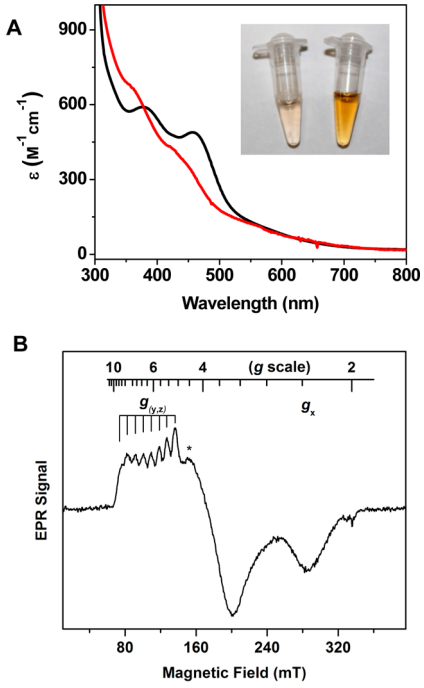

Figure 4. (A) UV−vis spectra of Co(II)-H228Y ACMSD (black) and Co(II)-substituted WT ACMSD (red). Photograph of the as-isolated Co-bound WT (left) and Co-H228Y (right) at the same protein concentrations are shown in the inset. (B) EPR spectra of Co(II)-H228Y ACMSD obtained at a 3 G modulation, 0.25 mW microwave power, and 10 K. The asterisk indicates a g = 4.27 signal from a small amount of Fe ion present in the sample due to a change in the metal preference of H228Y.

different from that of the WT protein, i.e., 2.343 versus 2.613, indicating that the ligand geometry around the metal ion in H228Y is different from that of the WT enzyme.[4] The optical and EPR data suggest that the high-spin cobalt center in brown H228Y is distinct from the cobalt center in the wild-type enzyme. The spectral features are most reminiscent of high-spin five-coordinate cobalt centers with square pyramidal geometry, such as that found in inhibitor derivatives of cobalt carbonic anhydrase.[65]

X-ray Crystal Structure. While the spectroscopic data strongly suggest a tyrosinate ligation to Fe in the as-isolated H228Y protein, it remains unclear whether Tyr228 is a metal ligand in Co(II)-substituted H228Y. The zinc-containing mutants do not have chromophore or EPR features. To observe directly what changes at the enzyme active site arise from the point mutation and metal substitution, we obtained single crystals from the as-isolated Fe(III)-H228Y, Co(II)-substituted H228Y, Zn(II)-substituted H228Y, and Zn(II)-reconstituted H228G proteins. The X-ray crystal structures of Fe(III)-H228Y (2.8 Å, PDB entry 4ERG), Co(II)-H228Y (2.4 Å resolution, PDB entry 4ERA), and Zn(II)-H228G (2.6 Å, PDB entry 4EPK) were determined in the $P4_22_12$ space group, while the structure of Zn(II)-H228Y (2.0 Å, PDB entry 4ERI) was determined in the $C2$ space group. Data collection and refinement statistics are listed in Table 2. Figure 5 shows the superimposition of the four structures we determined against the previously reported WT Zn(II)-ACMSD and Co(II)-substituted ACMSD data. As previously seen in the wild-type enzyme, the mutants of *Pf*ACMSD exhibit a homodimeric quaternary structure. The substitution of His228 with either Tyr or Gly has little impact on the folding of the overall TIM-barrel scaffold, regardless of the identity of the metal. The circular dichroism spectra of these variants were nearly identical to that of the WT enzyme (not shown), consistent with the structural data. In Figure 5, structural variations relative to WT ACMSD are highlighted in different colors. These structural differences are mainly observed in the previously defined

dx.doi.org/10.1021/bi300635b | *Biochemistry* 2012, 51, 5811−5821

Table 2. X-ray Crystallography Data Collection and Refinement Statistics

	Fe-H228Y	Co-H228Y	Zn-H228Y	Zn-H228G
		Data Collection		
detector type	MAR300 CCD	MAR225 CCD	MAR300 CCD	MAR300 CCD
source	APS, Sector 22-ID	APS, Sector 22-BM	APS, Sector 22-ID	APS, Sector 22-ID
space group	$P4_22_12$	$P4_22_12$	$C2$	$P4_22_12$
unit cell lengths (Å)	$a = b = 90.43$, $c = 167.53$	$a = b = 90.03$, $c = 167.31$	$a = 153.84$, $b = 48.56$, $c = 110.20$	$a = b = 91.50$, $c = 170.12$
unit cell angles (deg)	$\alpha = \beta = \gamma = 90$	$\alpha = \beta = \gamma = 90$	$\alpha = \gamma = 90$, $\beta = 126.89$	$\alpha = \beta = \gamma = 90$
wavelength (Å)	1.00	1.00	1.00	1.00
temperature (K)	100	100	100	100
resolution (Å)[a]	50.00−2.80 (2.85−2.80)	35.00−2.40 (2.44−2.40)	50.00−2.00 (2.03−2.00)	50.00−2.60 (2.64−2.60)
completeness (%)[a]	99.8 (99.8)	99.2 (94.1)	92.7 (54.7)	98.4 (68.7)
R_{merge} (%)[a,b]	10.1 (69.7)	10.1 (61.0)	6.1 (22.8)	7.7 (65.6)
$I/\sigma I$[a]	60.8 (2.5)	40.5 (2.9)	51.1 (6.0)	63.1 (1.9)
multiplicity[a]	24.2 (9.8)	13.9 (9.6)	6.3 (3.4)	18.6 (7.2)
		Refinement		
resolution (Å)	2.8	2.4	2.0	2.6
no. of reflections (working/test)	17041/915	26155/1382	41014/2073	22859/1173
R_{work} (%)[c]	19.9	21.5	20.5	20.8
R_{free} (%)[d]	27.3	29.5	25.6	28.1
no. of protein atoms	5194	5194	5194	5153
no. of ligand atoms	2	2	3	3
no. of solvent sites	9	88	209	32
average B factor (Å^2)				
protein	75.4	57.9	45.6	65.2
metal ion at active site (Fe, Co, or Zn)	69.5	46.2	35.3	56.7
Mg(II) ion	NA	NA	65.1	80.6
solvent	72.2	50.9	41.5	50.7
Ramachandran statistics[e] (%)				
preferred	93.48	92.73	94.52	91.78
allowed	5.61	5.61	4.72	7.61
root-mean-square deviation				
bond lengths (Å)	0.011	0.011	0.008	0.009
bond angles (deg)	1.299	1.464	1.098	1.204
PDB entry	4ERG	4ERA	4ERI	4EPK

[a]Values in parentheses are for the highest-resolution shell. [b]$R_{merge} = \sum_i |I_{hkl,i} - \langle I_{hkl}\rangle| / \sum_{hkl}\sum_i I_{hkl,i}$, where $I_{hkl,i}$ is the observed intensity and $\langle I_{hkl}\rangle$ is the average intensity of multiple measurements. [c]$R_{work} = \sum||F_o| - |F_c|| / \sum|F_o|$, where $|F_o|$ is the observed structure factor amplitude and $|F_c|$ is the calculated structure factor amplitude. [d]R_{free} is the R factor based on 5% of the data excluded from refinement. [e]Based on values attained from refinement validation options in COOT.

mobile insertion domain, which is more flexible than other parts of the structure.[18] Limited structural differences in a few loop regions are observed because of changes in metal ligation in the metal-substituted mutants. Therefore, we conclude that no significant change in secondary structure was introduced because of the mutation and metal substitution. The organization of amino acid residues surrounding the metal center is very similar in all four structures with one exception, one of the metal ligands, Asp294, which tilts toward the imidazole ring of His9 to various degrees (Figure 6).

Inspection of the metal center shows that Tyr228 is a metal ligand in all three H228Y mutant proteins (Figure 6), with Tyr−metal bond lengths of 2.13, 2.12, and 2.41 Å in chain A and 2.26, 2.16, and 2.44 Å in chain B in the Co-, Fe-, and Zn-H228Y structures, respectively. It would appear that the interaction between the Zn ion and the Tyr228 residue is weaker than the corresponding interactions with Fe and Co. Nonetheless, the angles among the Tyr228 plane, the phenolic oxygen, and the metal, including zinc, are well within the range of typical metal−ligand angular orientations (110−140°) reported in biological systems (130.2°, 137.3°, and 128.7° in chain A and 129.7°, 132.5°, and 122.6° in chain B in the Co-, Fe-, and Zn-H228Y structures, respectively).[66] Hence, the prediction of Tyr228 ligation by our spectroscopic work is confirmed by these as-isolated and metal-substituted H228Y structures. It should be noted that the metal center in chain B in the mutant structures shows a noticeable degree of disorder. This was the same as previously observed in the as-isolated and cobalt-substituted wild-type ACMSD structures (PDB entries 2HBV and 2HBX, respectively).[18]

The most significant structural difference with respect to the WT structure is that the water ligand is missing from the metal center in Fe(III)-H228Y, Co(II)-substituted H228Y, and Zn(II)-reconstituted H228G proteins. Modeling of the omit maps (Figure S2 of the Supporting Information) shows the electron density can be fit only by the metal ion in these structures. However, the resolution is not sufficiently high for assignment of the solvent content in the Fe(III)-H228Y and Zn(II)-H228G data sets, and the missing water ligand cannot be reliably identified on the basis of these structures. In contrast, Zn(II)-H228Y and Co(II)-substituted H228Y structures contain a reasonable amount of water molecules. The

dx.doi.org/10.1021/bi300635b | Biochemistry 2012, 51, 5811−5821

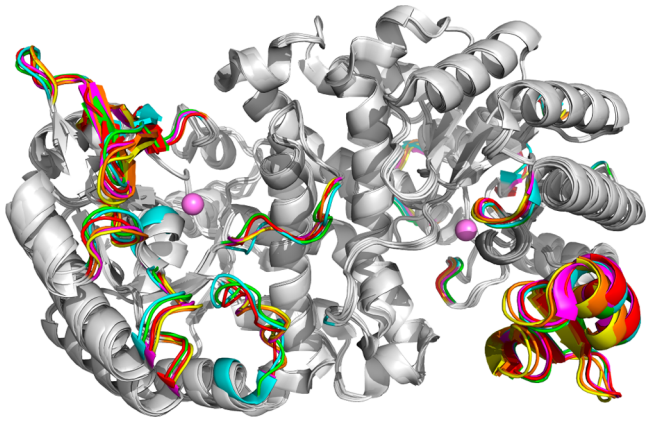

Figure 5. Superimposed overall structure of WT Zn(II)-ACMSD (blue, PDB entry 2HBV), WT Co(II)-ACMSD (magenta, PDB entry 2HBX), Fe(III)-H228Y ACMSD (orange, PDB entry 4ERG), Co(II)-H228Y (yellow, PDB entry 4ERA), Zn(II)-H228Y (green, PDB entry 4ERI), and Zn(II)-H228G (red, PDB entry 4EPK). The well-overlaid structural components are colored gray. Metal ions are represented as violet spheres. This figure was produced using PyMOL (http://www.pymol.org/).

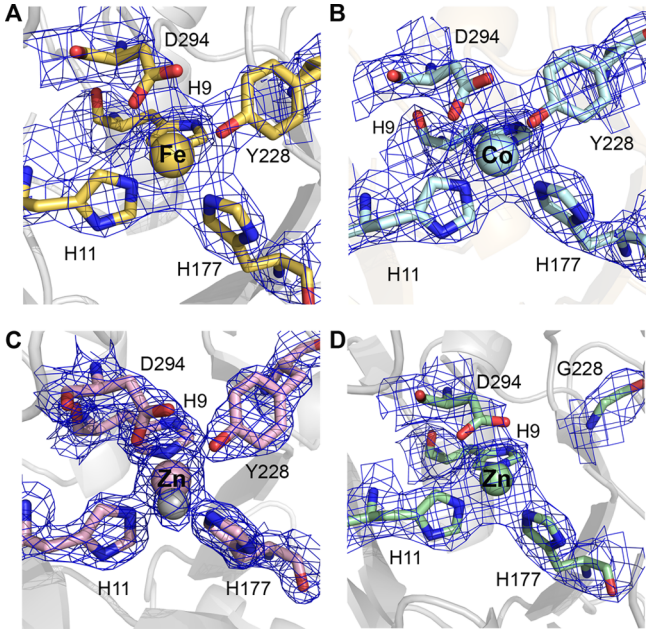

Figure 6. Active site structure of (A) as-isolated Fe(III)-H228Y, (B) Co(II)-substituted H228Y, (C) Zn(II)-H228Y, and (D) Zn(II)-substituted H228G. The $2F_o - F_c$ electron densities are taken from chain A and contoured at 1.5σ. The larger spheres represent metal ions. The smaller gray sphere in panel C represents a water molecule, which is weakly bound to the zinc ion (2.44 Å) as compared to the zinc−water ligand distance of 2.04 Å in the wild-type enzyme (PDB entry 2HBV). Such a water ligand is missing from the metal center in all other H228G and H228Y structures.

water ligand is missing from the cobalt structure, whereas the water ligand is still present in the Zn(II)-substituted H228Y structure but at a much greater distance from the metal, 2.44 Å in chain A and 2.38 Å in chain B from the zinc ion as compared to 2.05 and 2.07 Å, respectively, in the WT Zn-ACMSD structure. Our EPR, resonance Raman, and optical data suggest a low coordination number in the Co(II)- and Fe(III)-H228Y metal center. Taken together, it is likely that the water ligand is missing, or dissociated, from the metal center in Co(II)- and Fe(III)-H228Y mutants. Moreover, the hydrogen bonding network that potentially activates the water ligand is significantly altered. In the WT Zn-ACMSD crystal structure, the water ligand hydrogen bonds to both His228 and Asp294, while in the H228Y mutant, the distance between Asp294 and the water ligand is elongated to 3.60 Å in chain A and 3.67 Å in chain B, compared to distances of 2.88 and 3.33 Å, respectively, in WT Zn-ACMSD. In the H228G structure, the metal center is still five-coordinate even though the water ligand is absent. Asp294 becomes a bidentate ligand to the metal ion. From the H228G structure and the three H228Y structures, we conclude that His228 plays an important role in metal ion recruitment and in the maintenance of the position of the water ligand.

DISCUSSION

His228 Is a Major Determinant of Metal Ion Selectivity in *Pf*ACMSD. ACMSD was thought to be a cofactor-free enzyme for approximately 50 years until we found that many divalent transition metal ions can effectively activate it.[4] In a subsequent study, we found that the as-isolated protein contains only zinc ion.[18] However, the molecular basis of metal selectivity in proteins is generally poorly understood, and the preference for zinc within the active site of ACMSD has remained a mystery prior to this work. In the work presented here, a point mutation of a second coordination sphere His228 residue to Gly or Tyr is described to change *Pf*ACMSD's metal ion selectivity from Zn to Fe ion. In general, the primary control of metal selectivity in proteins should be the metal-binding ligand set. The fact that a single site mutation on a non-metal ligand residue changes metal selectivity in a protein is a surprising result. To the best of our knowledge, the finding described in this work for the metal selection role of a second coordination sphere residue is only the second example in the literature. Previously, mutation of a conserved glutamate in *E. coli* manganese superoxide dismutase has been shown to change metal preference to Fe ion.[67] In all other documented cases, the residue identified as affecting metal selectivity is a metal ligand. The lesson learned from *Pf*ACMSD His228 is anticipated to improve our understanding of metal ion selectivity in proteins and expand the scope of roles histidine plays in the enzyme active site.

Origin of the Blue Color in H228Y. To understand the underlying reason for the loss of enzyme activity due to mutation of His228, a spectroscopic study was performed to interrogate the metal center's chemical and electronic structure in H228Y. The optical and NBT staining data suggest the ligation of Tyr228 to the Fe ion in the as-isolated Fe(III)-H228Y, and this notion is further supported by our resonance Raman results. These data also eliminate the possibility of post-translational modification of Tyr228 to a DOPA.

Role of His228 in Maintaining the Hydrolytic Water Ligand for Catalysis. His228 attracted our attention because it is a strictly conserved active site residue. It lies on the opposite side of the presumed substrate binding pocket.[18,20] A previous structural study has revealed the conformational diversity of this active site residue.[18] In the work presented here, His228 was mutated to tyrosine and glycine. In line with our expectations, neither of the protein variants had a measurable catalytic activity, regardless of which metal was incorporated into the active site. The biochemical and spectroscopic data suggest that the loss of catalytic activity is, in large part, due to the missing histidine that acts as an acid/

dx.doi.org/10.1021/bi300635b | *Biochemistry* 2012, 51, 5811−5821

base catalyst and the loss of the water ligand. Thus, a dual role of His228 is revealed; i.e., it stabilizes the water ligand while it plays an important role in the metal selectivity of the enzyme.

Tyrosinate ligation to the metal center was identified by resonance Raman spectroscopy and further supported by the EPR data. Fe(III)-tyrosinate LMCT bands range from 410 to 600 nm where the energy of the LMCT can be correlated to the Lewis acidity and the redox potential of the Fe(III) center and give additional information about the nature of the other coordinating ligands. The low-energy LMCT band of H228Y-Fe(III)-ACMSD (595 nm) is suggestive of a very Lewis acidic metal center with very weak field ligands. A low coordination number (<6) may lead to a Lewis acidic Fe(III) and a low-energy LMCT. The UV−vis absorption spectra of both WT and Co(II)-substituted H228Y suggest five-coordinate metal centers. Therefore, the water ligand in the wild-type enzyme is likely replaced by the Tyr228 residue in the mutant. In the crystal structures of H228Y proteins loaded with three different metal ions, Tyr228 is a metal ligand. The spectroscopic data and the crystallographic results are consistent with each other.

A water ligand is observed in all published structures of ACMSD, including Co(II)- and Zn(II)-*Pf*ACMSD, as well as Zn(II)-hACMSD proteins. Such a water ligand is also present in other members of the ACMSD subfamily, including 4-oxalomesaconate hydratase, and γ-resorcylate decarboxylase.[18,68,69] The structures of Fe(III)-H228Y, Co(II)-H228Y, and H228G are the first structures determined that do not show a water ligand, while Zn(II)-H228Y shows a weakly bound water ligand with a longer distance to the metal center compared to that of the WT protein. Because of its weak binding to the Zn center, the pK_a of the water ligand in Zn(II)-H228Y may not be decreased as effectively as in the WT proteins by coordination to the zinc ion. Cobalt and zinc ions are particularly strong Lewis acids and can dramatically reduce the pK_a of bound water ligands. In a well-established example of carbonic anhydrase, the bound Zn(II) ion decreases the pK_a of its water ligand from 15.7 to 7.[70−72] Catalysis ensues from this zinc activation of its bound water. His228 is strictly conserved within all known ACMSD amino acid sequences, and in all available structures of the enzyme, this residue is within hydrogen bonding distance of the water ligand. The primary role of this His228 is proposed to be deprotonation of the metal-bound water so that a hydroxide ion can be generated as an active site nucleophile at pH ∼6−7, the optimal pH range for ACMSD. Although the hydroxide attack mechanism model shown in Scheme 1 for ACMSD is distinct from those of other metal-dependent decarboxylases, it shares common features with the established mechanisms in the amidohydrolase superfamily.[2]

The results described in this work are consistent with our working model of the ACMSD reaction (Scheme 1). In the working mechanistic model shown in Scheme 1, the metal-bound water molecule is deprotonated to the hydroxide anion (OH^-) with the assistance of His228, which is acting as a general acid/base catalyst to deprotonate the zinc-bound water molecule for attack on the substrate. The hydroxide ion performs a nucleophilic attack on the C2═C3 bond of ACMS with concomitant protonation at C3. Essentially, a water molecule is added across the double bond with the hydroxyl group at C2 and the new proton at C3, generating a substrate-based tetrahedral intermediate. Collapse of the tetrahedral intermediate initiates the decarboxylation and produces α-aminomuconate-ε-semialdehyde and regenerates the metal center. This decarboxylation model follows a hydrolytic mechanism consistent with the mechanistic paradigm of the amidohydrolase superfamily.

■ ASSOCIATED CONTENT

Ⓢ Supporting Information

NBT staining test (Figure S1) and omit maps of the meter center in the X-ray crystal structure of His228 mutants (Figure S2). This material is available free of charge via the Internet at http://pubs.acs.org.

■ AUTHOR INFORMATION

Corresponding Author

*Department of Chemistry, Georgia State University, P.O. Box 4098, Atlanta, GA 30303. Telephone: (404) 413-5532. Fax: (404) 413-5505. E-mail: Feradical@gsu.edu.

Present Address

⊥Division of Comparative Pathology, Tulane National Primate Research Center, 18703 Three Rivers Rd., Covington, LA 70433.

Author Contributions

L.H., A.J.F., Y.C., and T.L. contributed equally to this work.

Funding

Supported in part by National Science Foundation Grant MCB-0843537 (A.L.), National Institutes of Health (NIH) Grants GM 038767 (L.Q.) and GM 056824 (J.P.H.), the Japanese strategic projects to support the formation of research bases at private universities (matching fund subsidy from MEXT, 2008−2012), and the University of Minnesota Chemical Biology Initiative in conjunction with NIH-supported Chemistry Biology Interface Training Grant GM 08700 (A.J.F.).

Notes

The authors declare no competing financial interest.

■ ACKNOWLEDGMENTS

We thank Dr. Victor L. Davidson for the generous gift of a control sample used in the quinone-based NBT staining and Drs. Xiaodong Cheng and John Horton for allowing us to use the X-ray crystal screening facility at Emory University on a fee-based contract. X-ray data were collected at the Southeast Regional Collaborative Access Team (SER-CAT) 22-ID and 22-BM beamlines at the Advanced Photon Source (Argonne National Laboratory, Argonne, IL). We thank Dr. Bi-Cheng Wang and the SER-CAT staff at section 22 for assistance with remote data collections. Use of the Advanced Photon Source was supported by the U.S. Department of Energy, Office of Science, Office of Basic Energy Sciences, under Contract W-31-109-Eng-38.

■ ABBREVIATIONS

ACMS, α-amino-β-carboxymuconate-ε-semialdehyde; ACMSD, ACMS decarboxylase; *Pf*ACMSD, ACMSD from *P. fluorescens*; EPR, electronic paramagnetic resonance spectroscopy; HPPD, (4-hydroxyphenyl)pyruvate dioxygenase; LMCT, ligand-to-metal charge transfer; ICP-OES, coupled plasma optical emission spectroscopy; WT, wild-type; PDB, Protein Data Bank.

■ REFERENCES

(1) Rebek, J. (1990) On the structure of histidine and its role in enzyme active sites. *Struct. Chem. 1*, 129−131.

(2) Seibert, C. M., and Raushel, F. M. (2005) Structural and catalytic diversity within the amidohydrolase superfamily. *Biochemistry 44*, 6383−6391.
(3) Liu, A., Li, T., and Fu, R. (2007) Amidohydrolase Superfamily. In *Encyclopedia of Life Sciences* (Frey, P. A., Ed.) John Wiley & Sons, Ltd., New York (http://dx.doi.org/10.1002/9780470015902.a9780470020546).
(4) Li, T., Walker, A. L., Iwaki, H., Hasegawa, Y., and Liu, A. (2005) Kinetic and spectroscopic characterization of ACMSD from *Pseudomonas fluorescens* reveals a pentacoordinate mononuclear metallocofactor. *J. Am. Chem. Soc. 127*, 12282−12290.
(5) Li, T., Iwaki, H., Fu, R., Hasegawa, Y., Zhang, H., and Liu, A. (2006) α-Amino-β-carboxymuconic-ε-semialdehyde decarboxylase (ACMSD) is a new member of the amidohydrolase superfamily. *Biochemistry 45*, 6628−6634.
(6) Liu, A., and Zhang, H. (2006) Transition metal-catalyzed nonoxidative decarboxylation reactions. *Biochemistry 45*, 10407−10411.
(7) Nishizuka, Y., Ichiyama, A., and Hayaishi, O. (1970) Metabolism of the benzene ring of tryptophan. *Methods Enzymol. 17*, 463−466.
(8) Muraki, T., Taki, M., Hasegawa, Y., Iwaki, H., and Lau, P. C. (2003) Prokaryotic homologs of the eukaryotic 3-hydroxyanthranilate 3,4-dioxygenase and 2-amino-3-carboxymuconate-6-semialdehyde decarboxylase in the 2-nitrobenzoate degradation pathway of *Pseudomonas fluorescens* strain KU-7. *Appl. Environ. Microbiol. 69*, 1564−1572.
(9) Kurnasov, O., Goral, V., Colabroy, K., Gerdes, S., Anantha, S., Osterman, A., and Begley, T. P. (2003) NAD biosynthesis: Identification of the tryptophan to quinolinate pathway in bacteria. *Chem. Biol. 10*, 1195−1204.
(10) Colabroy, K. L., and Begley, T. P. (2005) Tryptophan catabolism: Identification and characterization of a new degradative pathway. *J. Bacteriol. 187*, 7866−7869.
(11) Mehler, A. H. (1964) Nicotinic acid biosynthesis: Control by an enzyme that competes with a spontaneous reaction. *Science 145*, 817−819.
(12) Stone, T. W., and Darlington, L. G. (2002) Endogenous kynurenines as targets for drug discovery and development. *Nat. Rev. Drug Discovery 1*, 609−620.
(13) Reinhard, J. F., Jr. (2004) Pharmacological manipulation of brain kynurenine metabolism. *Ann. N.Y. Acad. Sci. 1035*, 335−349.
(14) Guillemin, G. J., Williams, K. R., Smith, D. G., Smythe, G. A., Croitoru-Lamoury, J., and Brew, B. J. (2003) Quinolinic acid in the pathogenesis of alzheimer's disease. *Development in Tryptophan Serotonin Metabolism 527*, 167−176.
(15) Guidetti, P., and Schwarcz, R. (2003) 3-Hydroxykynurenine and quinolinate: Pathogenic synergism in early grade huntington's disease? *Development in Tryptophan and Serotonin Metabolism 527*, 137−145.
(16) Schwarcz, R. (2004) The kynurenine pathway of tryptophan degradation as a drug target. *Curr. Opin. Pharmacol. 4*, 12−17.
(17) Mehler, A. H. (1956) Formation of picolinic and quinolinic acids following enzymatic oxidation of 3-hydroxyanthranilic acid. *J. Biol. Chem. 218*, 241−254.
(18) Martynowski, D., Eyobo, Y., Li, T., Yang, K., Liu, A., and Zhang, H. (2006) Crystal structure of α-amino-β-carboxymuconic-ε-semialdehyde decarboxylase (ACMSD): Insight into the active site and catalytic mechanism of a novel decarboxylation reaction. *Biochemistry 45*, 10412−10421.
(19) Li, T., Ma, J., Hosler, J. P., Davidson, V. L., and Liu, A. (2007) Detection of transient intermediates in the metal-dependent nonoxidative decarboxylation catalyzed by α-amino-β-carboxymuconic-ε-semialdehyde decarboxylase. *J. Am. Chem. Soc. 129*, 9278−9279.
(20) Garavaglia, S., Perozzi, S., Galeazzi, L., Raffaelli, N., and Rizzi, M. (2009) The crystal structure of human α-amino-β-carboxymuconic-ε-semialdehyde decarboxylase in complex with 1,3-dihydroxyacetone-phosphate suggests a regulatory link between NAD synthesis and glycolysis. *FEBS J. 276*, 6615−6623.
(21) Horton, R. M. (1995) PCR-mediated recombination and mutagenesis. SOEing together tailor-made genes. *Mol. Biotechnol. 3*, 93−99.
(22) Otto, J. J. (1993) Immunoblotting. *Methods Cell Biol. 37*, 105−117.
(23) Paz, M. A., Fluckiger, R., Boak, A., Kagan, H. M., and Gallop, P. M. (1991) Specific detection of quinoproteins by redox-cycling staining. *J. Biol. Chem. 266*, 689−692.
(24) Yan, F., Li, T., Lipscomb, J. D., Liu, A., and Liu, H. W. (2005) Site-directed mutagenesis and spectroscopic studies of the iron-binding site of (*S*)-2-hydroxypropylphosphonic acid epoxidase. *Arch. Biochem. Biophys. 442*, 82−91.
(25) Chen, L. Y., Doi, N., Durley, R. C. E., Chistoserdov, A. Y., Lidstrom, M. E., Davidson, V. L., and Mathews, F. S. (1998) Refined crystal structure of methylamine dehydrogenase from paracoccus denitrificans at 1.75 Å resolution. *J. Mol. Biol. 276*, 131−149.
(26) Otwinowski, Z., and Minor, W. (1997) Processing of X-ray diffraction data collected in oscillation mode. *Methods Enzymol. 276*, 307−326.
(27) Vagin, A., and Teplyakov, A. (2010) Molecular replacement with MOLRE. *Acta Crystallogr. D66*, 22−25.
(28) Bailey, S. (1994) The Ccp4 Suite: Programs for protein crystallography. *Acta Crystallogr. D50*, 760−763.
(29) Murshudov, G. N., Vagin, A. A., and Dodson, E. J. (1997) Refinement of macromolecular structures by the maximum-likelihood method. *Acta Crystallogr. D53*, 240−255.
(30) Emsley, P., and Cowtan, K. (2004) Coot: Model-building tools for molecular graphics. *Acta Crystallogr. D60*, 2126−2132.
(31) Muller, I., Stuckl, C., Wakely, J., Kertesz, M., and Uson, I. (2005) Succinate complex crystal structures of the α-ketoglutarate-dependent dioxygenase AtsK: Steric aspects of enzyme self-hydroxlation. *J. Biol. Chem. 280*, 5716−5723.
(32) Ryle, M. J., Koehntop, K. D., Liu, A. M., Que, L., and Hausinger, R. P. (2003) Interconversion of two oxidized forms of taurine/α-ketoglutarate dioxygenase, a non-heme iron hydroxylase: Evidence for bicarbonate binding. *Proc. Natl. Acad. Sci. U.S.A. 100*, 3790−3795.
(33) Davis, J. C., Lin, S. S., and Averill, B. A. (1981) Kinetics and optical spectroscopic studies on the purple acid phosphatase from beef spleen. *Biochemistry 20*, 4062−4067.
(34) Zambonelli, C., and Roberts, M. F. (2003) An iron-dependent bacterial phospholipase D reminiscent of purple acid phosphatases. *J. Biol. Chem. 278*, 13706−13711.
(35) Vainshtein, B. K., Melik-Adamyan, W. R., Barynin, V. V., Vagin, A. A., and Grebenko, A. I. (1981) Three-dimensional structure of the enzyme catalase. *Nature 293*, 411−412.
(36) Pyrz, J. W., Roe, A. L., Stern, L. J., and Que, L., Jr. (1985) Model studies of iron-tyrosinate proteins. *J. Am. Chem. Soc. 107*, 614−620.
(37) Bradley, F. C., Lindstedt, S., Lipscomb, J. D., Que, L., Jr., Roe, A. L., and Rundgren, M. (1986) 4-Hydroxyphenylpyruvate dioxygenase is an iron-tyrosinate protein. *J. Biol. Chem. 261*, 11693−11696.
(38) Davis, M. I., Orville, A. M., Neese, F., Zaleski, J. M., Lipscomb, J. D., and Solomon, E. I. (2002) Spectroscopic and electronic structure studies of protocatechuate 3,4-dioxygenase: Nature of tyrosinate-Fe(III) bonds and their contribution to reactivity. *J. Am. Chem. Soc. 124*, 602−614.
(39) Que, L., Jr. (1988) *Metal-tyrosinate proteins in biological applications of Raman spectroscopy: Resonance Raman spectra of heme and metalloproteins*, Wiley-Interscience, New York.
(40) Tomimatsu, Y., Kint, S., and Scherer, J. R. (1976) Resonance Raman spectra of iron(III)-, copper(II)-, cobalt(III)-, and manganese(III)-transferrins and of bis(2,4,6-trichlorophenolato)-diimidazolecopper(II) monohydrate, a possible model for copper(II) binding to transferrins. *Biochemistry 15*, 4918−4924.
(41) Siu, D. C. T., Orville, A. M., Lipscomb, J. D., Ohlendorf, D. H., and Que, L., Jr. (1992) Resonance Raman studies of the protocatechuate 3,4-dioxygenase from *Brevibacterium fuscum*. *Biochemistry 31*, 10443−10448.
(42) Que, L., Jr., Heistand, R. H., II, Mayer, R., and Roe, A. L. (1980) Resonance Raman studies of pyrocatechase-inhibitor complexes. *Biochemistry 19*, 2588−2593.
(43) Que, L., Jr., and Heistand, R. H., II (1979) Resonance Raman studies on pyrocatechase. *J. Am. Chem. Soc. 101*, 2219−2221.

(44) Heistand, R. H., II, Lauffer, R. B., Fikrig, E., and Que, L., Jr. (1982) Catecholate and phenolate iron complexes as models for the dioxygenases. *J. Am. Chem. Soc. 104*, 2789−2796.
(45) Gaber, B. P., Miskowski, V., and Spiro, T. G. (1974) Resonance Raman scattering from iron(III)- and copper(II)-transferrin and an iron(III) model compound. A spectroscopic interpretation of the transferrin binding site. *J. Am. Chem. Soc. 96*, 6868−6873.
(46) Aisen, P., and Leibman, A. (1972) Lactoferrin and transferrin: A comparative study. *Biochim. Biophys. Acta 257*, 314−323.
(47) Ainscough, E. W., Brodie, A. M., Plowman, J. E., Bloor, S. J., Loehr, J. S., and Loehr, T. M. (1980) Studies on human lactoferrin by electron paramagnetic resonance, fluorescence, and resonance Raman spectroscopy. *Biochemistry 19*, 4072−4079.
(48) Aasa, R., Malmstroem, B. G., and Saltman, P. (1963) The specific binding of iron(III) and copper(II) to transferrin and conalbumin. *Biochim. Biophys. Acta 75*, 203−222.
(49) Cox, D. D., Benkovic, S. J., Bloom, L. M., Bradley, F. C., Nelson, M. J., and Que, L., Jr. (1988) Catecholate LMCT bands as probes for the active sites of nonheme iron oxygenases. *J. Am. Chem. Soc. 110*, 2026−2032.
(50) Smith, J. J., Thomson, A. J., Proudfoot, A. E., and Wells, T. N. (1997) Identification of an Fe(III)-dihydroxyphenylalanine site in recombinant phosphomannose isomerase from *Candida albicans*. *Eur. J. Biochem. 244*, 325−333.
(51) Ryle, M. J., Liu, A., Muthukumaran, R. B., Ho, R. Y. N., Koehntop, K. D., McCracken, J., Que, L., Jr., and Hausinger, R. P. (2003) O_2- and α-ketoglutarate-dependent tyrosyl radical formation in TauD, an α-keto acid-dependent non-heme iron dioxygenase. *Biochemistry 42*, 1854−1862.
(52) Michaud-Soret, I., Andersson, K. K., Que, L., Jr., and Haavik, J. (1995) Resonance Raman studies of catecholate and phenolate complexes of recombinant human tyrosine hydroxylase. *Biochemistry 34*, 5504−5510.
(53) Farquhar, E. R., Koehntop, K. D., Emerson, J. P., and Que, L., Jr. (2005) Post-translational self-hydroxylation: A probe for oxygen activation mechanisms in non-heme iron enzymes. *Biochem. Biophys. Res. Commun. 338*, 230−239.
(54) Antanaitis, B. C., Strekas, T., and Aisen, P. (1982) Characterization of pink and purple uteroferrin by resonance Raman and CD spectroscopy. *J. Biol. Chem. 257*, 3766−3770.
(55) Siamwiza, M. N., Lord, R. C., Chen, M. C., Takamatsu, T., Harada, I., Matsuura, H., and Shimanouchi, T. (1975) Interpretation of the doublet at 850 and 830 cm^{-1} in the Raman spectra of tyrosyl residues in proteins and certain model compounds. *Biochemistry 14*, 4870−4876.
(56) Salama, S., Stong, J. D., Neilands, J. B., and Spiro, T. G. (1978) Electronic and resonance Raman spectra of iron(III) complexes of enterobactin, catechol, and *N*-methyl-2,3-dihydroxybenzamide. *Biochemistry 17*, 3781−3785.
(57) Gaber, B. P., Sheridan, J. P., Bazer, F. W., and Roberts, R. M. (1979) Resonance Raman scattering from uteroferrin, the purple glycoprotein of the porcine uterus. *J. Biol. Chem. 254*, 8340−8342.
(58) Lindstedt, S., and Rundgren, M. (1982) Blue color, metal content, and substrate binding in 4-hydroxyphenylpyruvate dioxygenase from *Pseudomonas* sp. strain P. J. 874. *J. Biol. Chem. 257*, 11922−11931.
(59) Serre, L., Sailland, A., Sy, D., Boudec, P., Rolland, A., Pebay-Peyroula, E., and Cohen-Addad, C. (1999) Crystal structure of *Pseudomonas fluorescens* 4-hydroxyphenylpyruvate dioxygenase: An enzyme involved in the tyrosine degradation pathway. *Structure 7*, 977−988.
(60) Loroesch, J., and Haase, W. (1986) Cobalt(II)-hemocyanin: A model for the cuprous deoxy protein giving evidence for a bridging ligand in the active site. *Biochemistry 25*, 5850−5857.
(61) Horrocks, W. D., Jr., Ishley, J. N., Holmquist, B., and Thompson, J. S. (1980) Structural and electronic mimics of the active site of cobalt(II)-substituted zinc metalloenzymes. *J. Inorg. Biochem. 12*, 131−141.
(62) Sellin, S., Eriksson, L. E., Aronsson, A. C., and Mannervik, B. (1983) Octahedral metal coordination in the active site of glyoxalase I as evidenced by the properties of Co(II)-glyoxalase I. *J. Biol. Chem. 258*, 2091−2093.
(63) Bertini, I., and Luchinat, C. (1984) High spin cobalt(II) as a probe for the investigation of metalloproteins. *Adv. Inorg. Biochem. 6*, 71−111.
(64) Seffernick, J. L., McTavish, H., Osborne, J. P., de Souza, M. L., Sadowsky, M. J., and Wackett, L. P. (2002) Atrazine chlorohydrolase from *Pseudomonas* sp. strain ADP is a metalloenzyme. *Biochemistry 41*, 14430−14437.
(65) Bencini, A., Bertini, I., Canti, G., Gatteschi, D., and Luchinat, C. (1981) The EPR spectra of the inhibitor derivatives of cobalt carbonic anhydrase. *J. Inorg. Biochem. 14*, 81−93.
(66) Holm, R. H., Kennepohl, P., and Solomon, E. I. (1996) Structural and functional aspects of metal sites in biology. *Chem. Rev. 96*, 2239−2314.
(67) Whittaker, M. M., and Whittaker, J. W. (1998) A glutamate bridge is essential for dimer stability and metal selectivity in manganese superoxide dismutase. *J. Biol. Chem. 273*, 22188−22193.
(68) Goto, M., Hayashi, H., Miyahara, I., Hirotsu, K., Yoshida, M., and Oikawa, T. (2006) Crystal structures of nonoxidative zinc-dependent 2,6-dihydroxybenzoate (γ-resorcylate) decarboxylase from *Rhizobium* sp. strain MTP-10005. *J. Biol. Chem. 281*, 34365−34373.
(69) Forouhar, F., Abashidze, M., Jayaraman, S., Cunningham, K., Ciao, M., Ma, L. C., Xiao, R., Acton, T. B., Montelione, G. T., Hunt, J. F., and Tong, L. (2007) Crystal structure of 4-oxalomesaconate hydratase, LigJ, from *Rhodopseudomonas palustris*, Northeast Structural Genomics target RpR66. RCSB Protein Data Bank entry 2GWG.
(70) Silverman, D. N., and Lindskog, S. (1988) The catalytic mechanism of carbonic anhydrase: Implications of a rate-limiting protolysis of water. *Acc. Chem. Res. 21*, 30−36.
(71) Sly, W. S., and Hu, P. Y. (1995) Human carbonic anhydrases and carbonic anhydrase deficiencies. *Annu. Rev. Biochem. 64*, 375−401.
(72) Woolley, P. (1975) Models for metal ion function in carbonic anhydrase. *Nature 258*, 677−682.
(73) Farquhar, E. R., Emerson, J. P., Koehntop, K. D., Reynolds, M. F., Trmcic, M., and Que, L., Jr. (2011) In vivo self-hydroxylation of an iron-substituted manganese-dependent extradiol cleaving catechol dioxygenase. *J. Biol. Inorg. Chem. 16*, 589−597.
(74) Koehntop, K. D., Marimanikkuppam, S., Ryle, M. J., Hausinger, R. P., and Que, L., Jr. (2006) Self-hydroxylation of taurine/α-ketoglutarate dioxygenase: Evidence for more than one oxygen activation mechanism. *J. Biol. Inorg. Chem. 11*, 63−72.